# Supplemental information

# Programmable selective acylation of saccharides

# mediated by carbene and boronic acid

**Wen-Xin Lv, Hang Chen, Xinglong Zhang, Chang Chin Ho, Yingguo Liu, Shuquan Wu, Haiqi Wang, Zhichao Jin, and Yonggui Robin Chi**

## 3. Density functional theory (DFT) calculations

### 3.1. Computational Methods

For conformational sampling of structures, Grimme's *crest* program,[6,7] which used metadynamics (MTD) with genetic z-matrix crossing (GC) performed at the GFN2-xTB[8–10] extended semiempirical tight-binding level of theory, was used. The resulting lowest energy structures were further optimized using global hybrid DFT functional M06-2X[6] with Karlsruhe-family double-ζ valence def2-SVP[12,13] basis set for all atoms as implemented in *Gaussian 16* rev. B.01.[14] Single point (SP) corrections were performed using M06-2X functional and def2-TZVP[12] basis set for all atoms. Minima and transition structures on the potential energy surface (PES) were confirmed as such by harmonic frequency analysis, showing respectively zero and one imaginary frequency. The implicit SMD continuum solvation model[15] for acetonitrile solvent was used to account for the effect of solvent on the potential energy surface. Gibbs energies were evaluated at 50°C, which was used in the experiments, using a quasi-RRHO treatment of vibrational entropies.[16] Vibrational entropies of frequencies below 100 cm$^{-1}$ were obtained according to a free rotor description, using a smooth damping function to interpolate between the two limiting descriptions.[17] The free energies were further corrected using standard concentration of 1 mol/L for gas-phase-to-solvent correction. All molecular structures are visualized using *PyMOL* software.[18]

### 3.2. Model systems

To understand how the interactions between the NHC and the boronic acids employed effect the regioselective O-acylation, we chose the model reactions in figure S36 for our computational studies. (1) Comparing Reactions 1 and 2, we aim to see how a difference in the substituent group in the boronic acid affects the regioselective outcome. (2) Comparing Reactions 3 and 4, which employ the same reaction conditions, except the sugar used, we aim to understand how sugar stereochemistry affects regioselective outcome. (3) Finally, comparing Reactions 4 and 5, where enantiomeric NHCs are used on the same sugar, we aim to understand how NHC chirality affects regioselective outcome.

We considered the key step of the hydroxyl group attacking the carbonyl group of the acyl azolium as this step is regio-determining. The mechanistic study of the full catalytic cycle for the present reaction is underway in our laboratories.
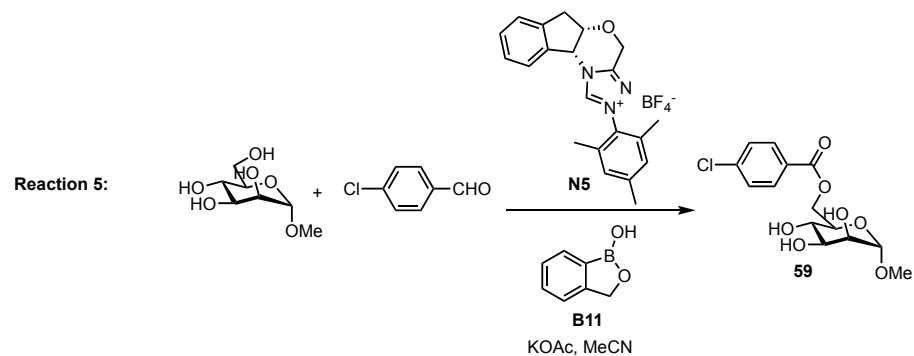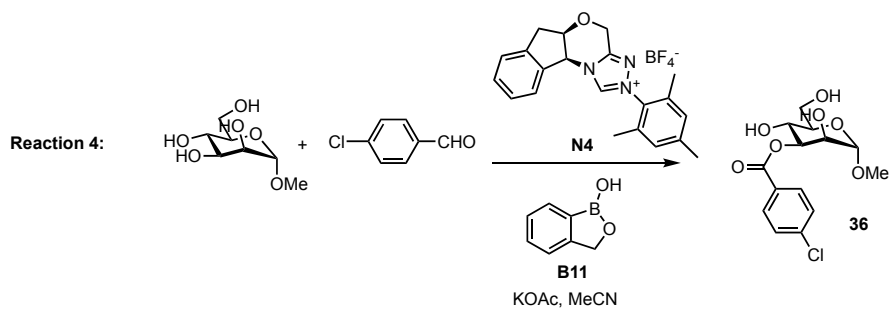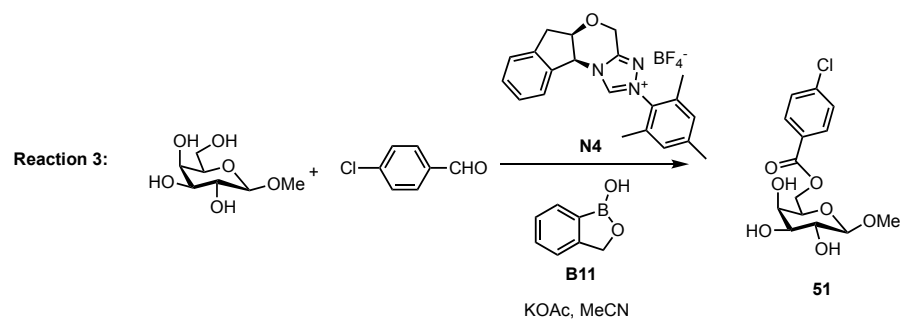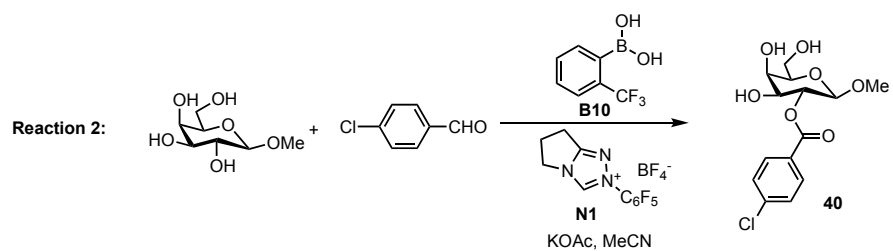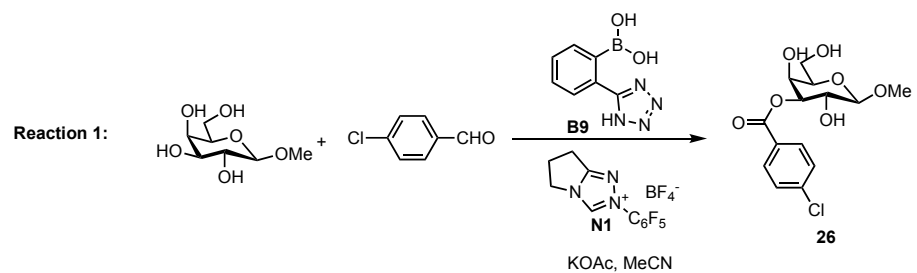
**Figure S36.** Model reactions for computational mechanistic studies.

### 3.3. Thermodynamics for the formation of boronic ester from the condensation reaction between boronic acid and sugar

We computed the Gibbs energy of reaction for the condensation between boronic acid and monosaccharide. The results are shown in Table S5. A general feature of our type of reaction, from the three reactions considered (where different monosaccharides, glucoside and galactoside, were used), is that the formation of boronic ester between the boronic acid and 4,6-diol of the sugar is exergonic (thermodynamically downhill), while that with 3,4-diol or 2,3-diol of the sugar are endergonic (thermodynamically uphill). This suggests that the formation with 4,6-diol of the sugar is favorable whereas the formations with 3,4-diol or 2,3-diol of the sugar are unfavorable. This means that under our reaction conditions where boronic acids can form boronic esters with monosaccharides, the hydroxyl groups at C4 and C6 will be involved in boronic ester formation, leaving hydroxyl groups at C2 and C3 exposed for subsequent acylation. We note that the hydroxyl groups on C4 and C6 can be of either *cis*- (as in galactoside) or *trans*-relationship (as in glucoside), without affecting this observation, as the C6 methylene group is flexible enough to ensure the formation of [6,6]-bicyclic rings in both cases. In addition, this observation is valid for all 3 boronic acids tested (**B1**, **B9**, **B10**, Table S5) and is likely to be valid for other boronic acids as well.
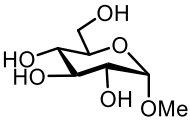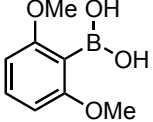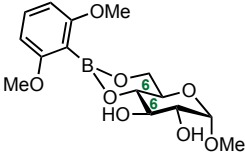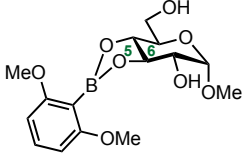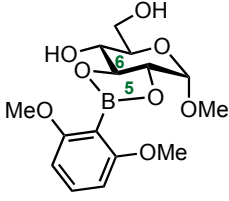
The formation of [6,6]-bicyclic boronic ester is more stable than that of [5,6]-bicyclic boronic ester. From Table S5, we can see that for the reaction involving galactoside and boronic acid **B9**, the formation of boronic ester **galactoside_B9_46diol** is 2.9 kcal mol$^{-1}$ and 8.8 kcal mol$^{-1}$ more stable than boronic esters **galactoside_B9_34diol** and **galactoside_B9_23diol**, respectively. Similarly, for the reaction between galactoside and boronic acid **B10**, the formation of boronic ester **galactoside_B10_46diol** is 6.0 kcal mol$^{-1}$ and 13.1 kcal mol$^{-1}$ more stable than boronic esters **galactoside_B10_34diol** and **galactoside_B10_23diol**, respectively. For the reaction between glucoside and boronic ester **B1**, the formation of boronic ester **glucoside_B1_46diol** is 9.6 kcal mol$^{-1}$ and 9.7 kcal mol$^{-1}$ more stable than boronic esters **glucoside_B1_34diol** and **glucoside_B1_23diol**, respectively. The boronic ester formed with 4,6-diol of the sugar is expected to be the dominant species present and subsequently takes part in the reaction. This is consistent with the experimental verification of the involvement of boronic ester formed with 4,6-diol of the sugar (intermediates **I** and **III**) in the reaction between glucoside **1** with NHC **N1** and boronic acid **B1** (section 2.6.2 and Figure S23).

We conclude that for our reaction protocols, where boronic acids employed can form boronic ester with the monosaccharide, the most stable adduct that reacts further in the reaction will be the boronic acid–4,6-diol adduct, leaving only exposed OH groups at C2 and C3 for selective acylation.

**Table S5.** Computed Gibbs energy of reaction for the condensation between monosaccharides and the boronic acids.
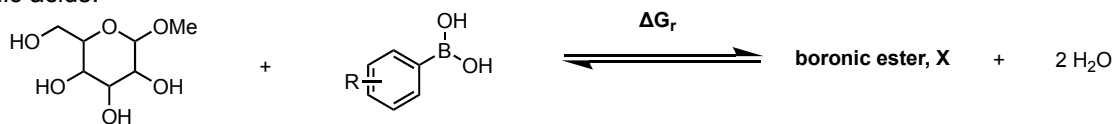


| sugar | boronic acid | boronic ester, X | $\Delta G_r$ / kcal mol$^{-1}$ |
|---|---|---|---|
| galactoside | B9 | galactoside_B9_46diol | -1.0 |
| | | galactoside_B9_34diol | 1.9 |
| | | galactoside_B9_23diol | 7.8 |
| galactoside | B10 | galactoside_B10_46diol | -5.0 |
| | | galactoside_B10_34diol | 1.0 |
| | | galactoside_B10_23diol | 8.1 |

| sugar | boronic acid | boronic ester, X | $\Delta G_r$ / kcal mol$^{-1}$ |
|---|---|---|---|
|   **glucoside** |   **B1** |   **glucoside_B1_46diol** | -5.1 |
| | |   **glucoside_B1_34diol** | 4.5 |
| | |   **glucoside_B1_23diol** | 4.6 |

## 3.4. Conformational analyses

To study the key regio-determining step of C–O bond formation between sugar hydroxyl group and the carbonyl C of acyl azolium intermediate, we need to consider the conformations of these transition states (TS). As such TS structures could not be located at the *xtb* level, we consider the conformations of the key intermediates as a proxy to the conformations in the regio-determining TSs as we expect the side group interactions to be similar in the intermediate and the TSs. In other words, favorable interactions such as π-π interactions and hydrogen bonding interactions in the intermediates are expected to be also present in the TSs.

Figure S37 shows the examples of the intermediates arising from the attack of the acyl azolium carbonyl group by the hydroxyl groups from the boronic ester (sugar). Two possibilities can occur, namely that a particular OH group can attack the carbonyl group from either the *(Si)*-face or the *(Re)*-face, giving rise to different stereoisomers with differing interactions among the side groups. Note that, although the interactions in these intermediates, and their corresponding TSs, are different, the subsequent loss of NHC as the oxyanion reforms the carbonyl group generates the same acylated sugar product in each case.
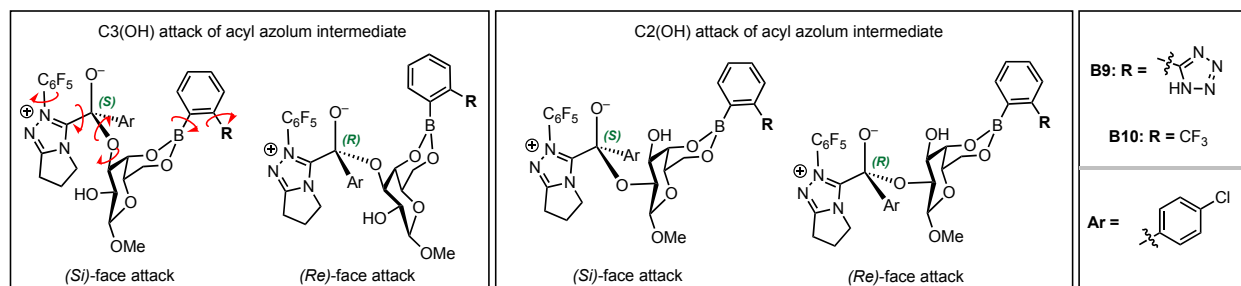


**Figure S37.** Example intermediate structures for conformational sampling. Example rotational degrees of freedom about single bonds are shown in red arrows.

Conformational sampling of the acyl azolium-sugar intermediate was performed using the *crest* program, as outlined in the methods section. An implicit solvation of acetonitrile using the generalized Born (GB) model with surface area (SA) contribution (GBSA) was included in the conformational sampling. The lowest energy conformer from this procedure was further optimized at DFT SMD(acetonitrile)-M06-2X/def2-TZVP//M06-2X/def2-SVP level of theory.

Figure S38 shows the DFT optimized structures. In **Reaction 1**, the NH group of the tetrazole ring of the boronic acid can form hydrogen bonding interaction with the oxyanion oxygen atom in formation of O(C3)–C(carbonyl) from either the *(Re)*- (**INT_gal_N1_B9_O3_Re**) or the *(Si)*-face attack (**INT_gal_N1_B9_O3_Si**). We can imagine that the formation of this hydrogen bonding strategically places the C(3)-OH group close to the carbonyl C=O group for productive C–O bond formation in the transition state, as illustrated in figure S39. For the formation of O(C2)–C(carbonyl) bond however, no such hydrogen bonding is possible due to the geometric restraints. In **INT_gal_N1_B9_O2_Si**, instead, a hydrogen bonding between the NH group of the tetrazole ring of the boronic acid and the anomeric oxygen atom is formed. This is in addition to the hydrogen bonding between C(3)-OH and the oxyanion oxygen atom. In **INT_gal_N1_B9_O2_Re**, however, no such interactions are possible, and only weak CH⋯O interaction is possible, thus explaining its much higher energy. In addition, the intermediates at C(3)-OH functionalization have π–π interactions that are absent in the C(2)-OH functionalization. These could be the origins for favoring C(3)-OH functionalized galactoside using the combination of NHC **N1** and boronic acid **B9**.

In **Reaction 2**, the most stable intermediate, **INT_gal_N1_B10_O2_Si**, benefits from various favorable interactions such as H bonding, CH⋯F and CF⋯π interactions. The H bond in this intermediate is stronger than the H bond in **INT_gal_N1_B10_O3_Re** ($\Delta\Delta G$ = 2.4 kcal mol$^{-1}$) as the former has a shortest distance of 1.50Å than the latter of 1.68Å (Figure S38). On the other hand, only weak interactions are present in **INT_gal_N1_B10_O2_Re** and **INT_gal_N1_B10_O3_Si** (CH⋯O and CF⋯π interactions), and there is no H bonding present, thus giving much higher relative energies (by 8.0 and 12.2 kcal mol$^{-1}$) than the most stable intermediate, **INT_gal_N1_B10_O2_Si.** Thus C(2)-OH functionalization of galactoside using the combination of NHC **N1** and boronic acid **B10** will be favored.

Comparing **Reactions 1** and **2**, we see that in **Reaction 2**, by changing the tetrazole ring of the boronic acid in **Reaction 1** to trifluoromethyl group in **Reaction 2**, no H-bonding from the boronic acid moiety via the NH group of the tetrazole ring is possible in **Reaction 2**, thus, no directed "delivery" of C(3)–OH bond to the carbonyl group for addition is possible.

In **Reactions 3, 4** and **5**, the monosaccharides are not protected by forming 4,6-boronato-monosaccharides as the boronic acids do not have two OH groups. Therefore, we consider the possibility of functionalization at all OH groups on the sugar substrate. For each intermediate, our independent *crest* conformer search converges to the lowest energy structures with same backbone orientations demonstrating similar interactions. For example, the interactions between the NHC moiety and the aryl ring of the acyl group in **INT_gal_N4_B11_Ox_Si** (**x**=2, 3, 4, 6) are all the same; similar observation can be made in **INT_gal_N4_B11_Ox_Re** (**x**=2, 3, 4, 6). This demonstrates that within each reaction, the acyl azolium intermediate forms specific interactions, priming the carbonyl group for the regioselective addition of a particular OH group of the monosaccharide over other OH groups depending on the monosaccharide chirality and the specific interactions that the monosaccharide can form with the acyl azolium intermediate.

Looking at all the lowest energy intermediates from either the (*Re*)- or (*Si*)-face attack of the carbonyl group of the acyl azolium intermediate by various OH groups, we can see that all these structures form favorable π⋯π interactions between the aryl ring of the acyl group and the mesityl group on the NHC. For **Reaction 3**, the (*Re*)-face attacks give more stable intermediates than the corresponding (*Si*)-face attack at each C(OH) functionalization whereas for **Reactions 4** and **5**, due to the different stereochemical orientation of the sugar and the chiral NHC, the (*Si*)-face attacks give more stable intermediates than the corresponding (*Re*)-face attack.

In **Reaction 3**, comparing the intermediates of different O-site functionalization (**INT_gal_N1_B10_Ox_Re** where **x**=2, 3, 4, 6), we see that **INT_gal_N4_B11_O6_Re** is the most stable, as this structure benefits from additional CH⋯O(anomeric) and CH⋯π interactions that are not present in the other 3 intermediates (**INT_gal_N1_B10_Ox_Re** where **x**=2, 3, 4). In addition, although H-bonding between one of the OH groups on the monosaccharide and the oxyanion oxygen atom is formed in all cases, the H-bonding is the strongest in **INT_gal_N4_B11_O6_Re** as evidenced by its much shorter H-bond length of (1.49Å) as compared to others (1.52Å in **INT_gal_N4_B11_O2_Re**, 1.57Å in **INT_gal_N4_B11_O4_Re**, and 1.65Å in **INT_gal_N4_B11_O3_Re**). This suggests that the TS for the regio-determining C–O(C(6)-OH) bond formation will likely benefit from similar interactions and give the lowest energy barriers, thus suggesting that C(6)-OH acylation is the most likely.

In **Reaction 4**, as compared to **Reaction 3**, now the mannoside used has different stereochemistry than the galactoside at C(2)-OH and C(4)-OH. Now, the most stable intermediates, and by extension the corresponding TSs leading to their formation, result from the (*Si*)-face attacks rather than the (*Re*)-face attacks in **Reaction 3**. The intermediate formed at C(3)-OH, **INT_man_N4_B11_O3_Si**, is the most stable, as it has two H-bonds and additional CH⋯O interaction and it has the strongest H-bond between the OH of manoside and oxyanion oxygen atom (bond distance of 1.52Å, Figure S38).

In **Reaction 5**, both the mannoside and the NHC have different stereochemistry from the galactoside and NHC used in **Reaction 3**. The most stable intermediates result from the (*Re*)-face attacks in **Reaction 3**, but from the (*Si*)-face attacks in **Reaction 5**. The double inversion of the stereochemistry in both the sugar and the NHC could explain why both **Reactions 3** and **5** favor the same OH-functionalization (both at C(6)-OH). For example, comparing **INT_gal_N4_B11_O6_Re** and **INT_man_N5_B11_O6_Si**, the most stable intermediate in **Reactions 3** and **Reactions 5**, respectively (Figure S38), the dihydroindene group of the NHC in both cases have similar orientation (point "downwards") as the sugar hydroxyl groups form various interactions. These two structures are almost mirror images, except where the stereochemistry of the sugar substrate differs. Both structures have the most favorable interactions than intermediates from other O-site functionalization within each of **Reactions 3** and **5**. The intermediate formed at C(3)-OH, **INT_man_N4_B11_O3_Si**, is the most stable, as it has two H-bonds and additional CH⋯O interaction and it has the strongest H-bond between the OH of mannoside and oxyanion oxygen atom (bond distance of 1.52Å, Figure S38).

When comparing **Reaction 5** to **Reaction 4**, both the intermediates resulting from the (*Si*)-face attack of the acyl azolium have lower energy than the corresponding intermediates from the (*Re*)-face attack. Comparing the intermediates from the (*Si*)-face attack in **Reactions 4** and **5** (Figure S38), we see that only the orientation of the dihydroindene group of the NHCs differs across these two reactions (e.g., **INT_man_N4_B11_Ox_Si vs INT_man_N5_B11_Ox_Si,** where **x**=2, 3, 4). This is consistent with our expectation, as the NHCs used are enantiomers (**N4** vs **N5**). This difference in the NHC side group

orientation favors different O-functionalization (C(6)-OH in **Reaction 5** vs C(3)-OH in **Reaction 4** due to the resultant differing electronic and steric interactions present.

Within **Reaction 5**, the most stable intermediate is **INT_man_N5_B11_O6_Si**, at C(6)-OH funnctionailzation. This intermediate forms three H-bonds whereas the other intermediates only have two H-bonds.

In summary, the regioselective outcome of sugar O-functionalization results from a combination of sterics (due to side groups of the NHCs/boronic acids used) and electronic interactions between the sugar OH/CH groups and the NHC side chains. The acyl azolium intermediate is stereogenic as the carbonyl carbon can be attacked by sugar hydroxyl group from either the (*Re*)- or (*Si*)-face. This provides opportunities for unique interactions as different OH groups attack into the carbonyl carbon of acyl azolium, thus giving unique regioselective outcomes.

| Reaction 1 | |
|---|---|
| **INT_gal_N1_B9_O2_Re** | **INT_gal_N1_B9_O2_Si** |
| ΔΔG = 5.7 | ΔΔG = 0.4 |
|  |  |
| **INT_gal_N1_B9_O3_Re** | **INT_gal_N1_B9_O3_Si** |
| ΔΔG = 1.7 | **ΔΔG = 0.0** |
|  |  |

| Reaction 2 | |
|---|---|
| **INT_gal_N1_B10_O2_Re** | **INT_gal_N1_B10_O2_Si** |
| ΔΔG = 8.0 | **ΔΔG = 0.0** |
| **INT_gal_N1_B10_O3_Re** | **INT_gal_N1_B10_O3_Si** |
| ΔΔG = 2.4 | ΔΔG = 12.2 |

| Reaction 3 | |
|---|---|
| **INT_gal_N4_B11_O2_Re** | **INT_gal_N4_B11_O2_Si** |
| ΔΔG = 6.0 | ΔΔG = 8.9 |
|  |  |
| **INT_gal_N4_B11_O3_Re** | **INT_gal_N4_B11_O3_Si** |
| ΔΔG = 7.3 | ΔΔG = 8.9 |
|  |  |
| **INT_gal_N4_B11_O4_Re** | **INT_gal_N4_B11_O4_Si** |
| ΔΔG = 9.5 | ΔΔG = 12.9 |
|  |  |

| INT_gal_N4_B11_O6_Re | INT_gal_N4_B11_O6_Si |
|:---:|:---:|
| **ΔΔG = 0.0** | ΔΔG = 6.1 |

| Reaction 4 | |
|---|---|
| **INT_man_N4_B11_O2_Re** | **INT_man_N4_B11_O2_Si** |
| ΔΔG = 4.4 | ΔΔG = 0.5 |
|  |  |
| **INT_man_N4_B11_O3_Re** | **INT_man_N4_B11_O3_Si** |
| ΔΔG = 6.0 | **ΔΔG = 0.0** |
|  |  |
| **INT_man_N4_B11_O4_Re** | **INT_man_N4_B11_O4_Si** |
| ΔΔG = 6.6 | ΔΔG = 0.5 |
|  |  |
| **INT_man_N4_B11_O6_Re** | **INT_man_N4_B11_O6_Si** |

| ΔΔG = 2.0 | ΔΔG = 2.0 |
|---|---|

| Reaction 5 | |
|---|---|
| **INT_man_N5_B11_O2_Re** | **INT_man_N5_B11_O2_Si** |
| ΔΔG = 5.5 | ΔΔG = 1.3 |
| **INT_man_N5_B11_O3_Re** | **INT_man_N5_B11_O3_Si** |
| ΔΔG = 7.5 | ΔΔG = 1.2 |
| **INT_man_N5_B11_O4_Re** | **INT_man_N5_B11_O4_Si** |
| ΔΔG = 6.7 | ΔΔG = 1.8 |

| INT_man_N5_B11_O6_Re | INT_man_N5_B11_O6_Si |
|---|---|
| ΔΔG = 5.0 | **ΔΔG = 0.0** |
|  |  |
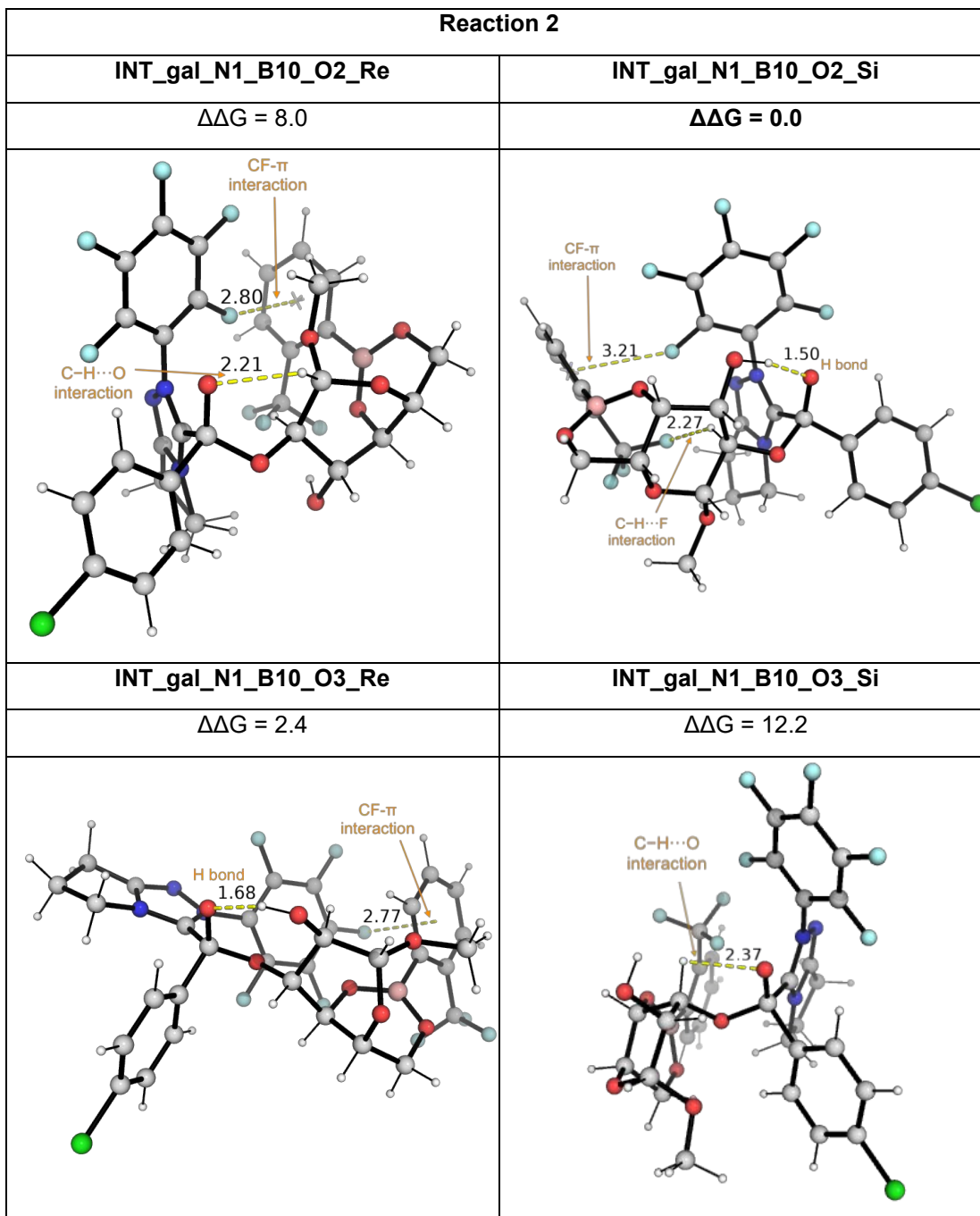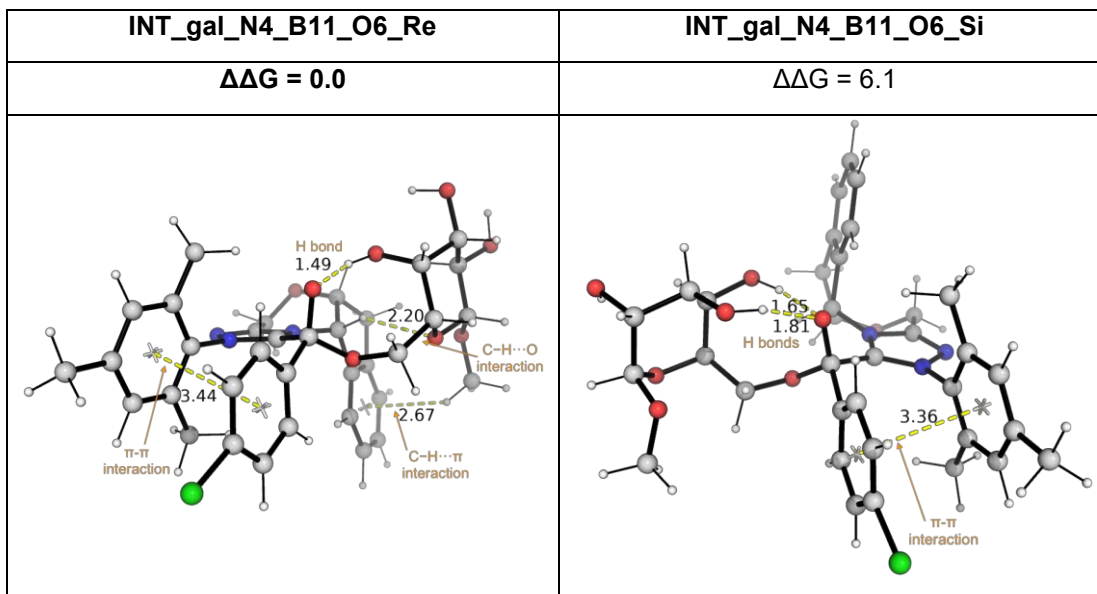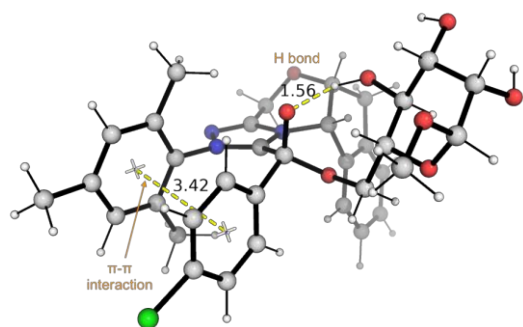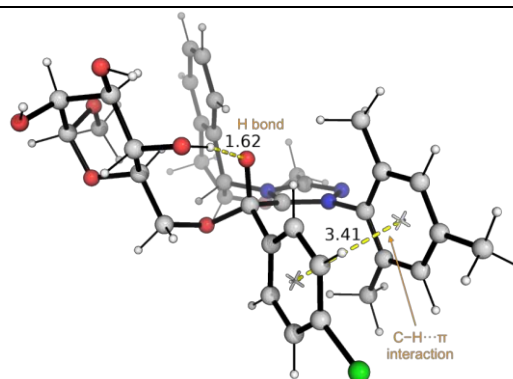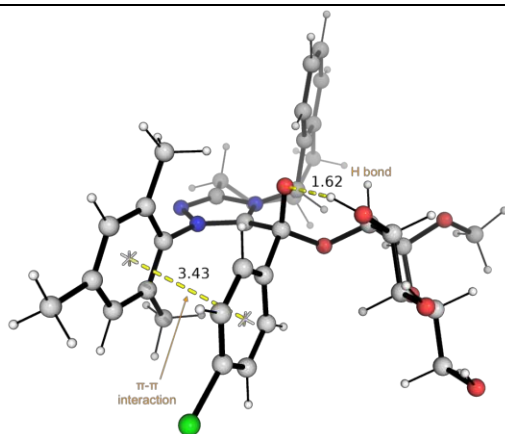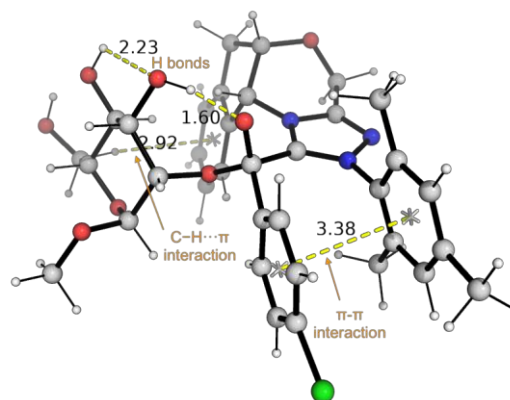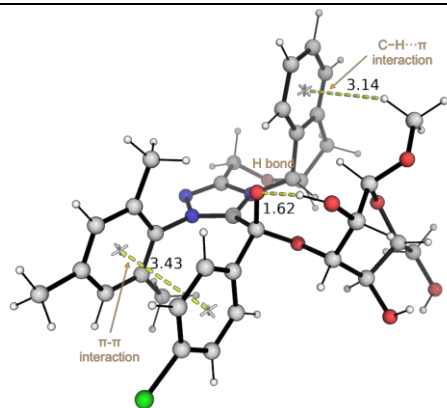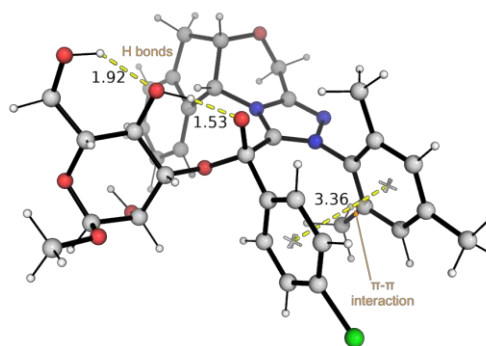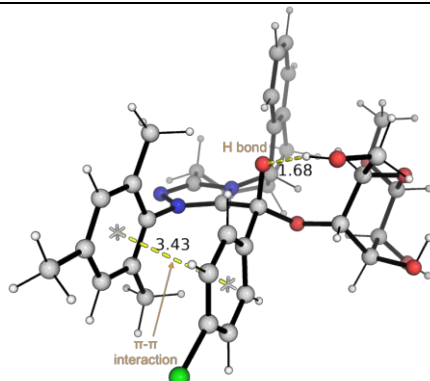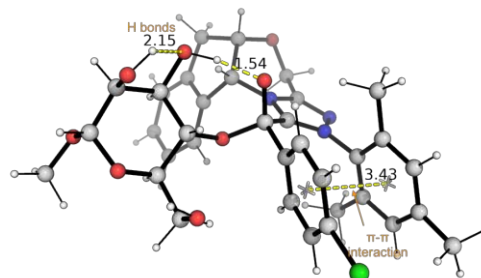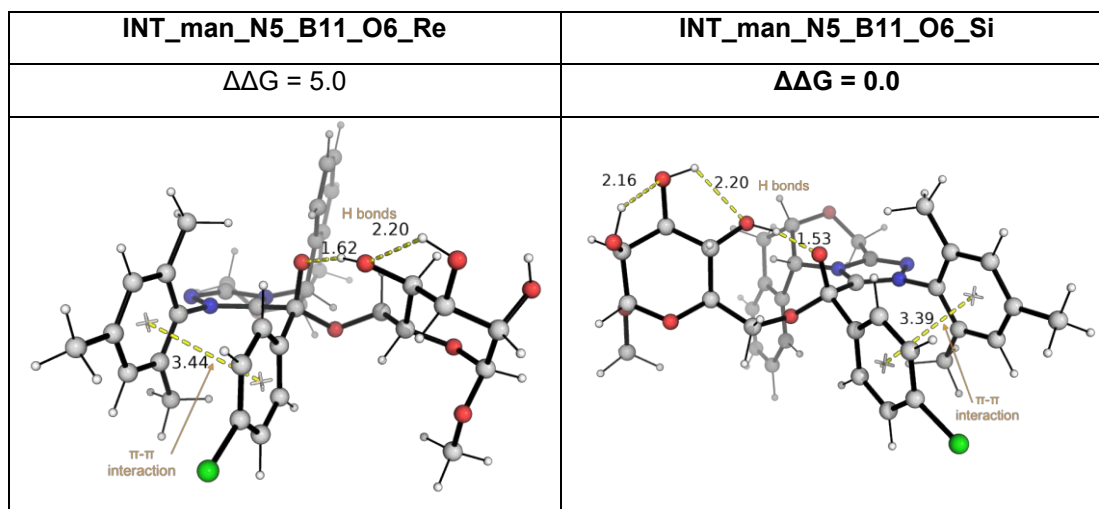
**Figure S38.** DFT optimized structures of the lowest energy conformers resulting from each of the reactions in figure S36. Relative Gibbs energy is taken with respect to the lowest energy conformer within each reaction.
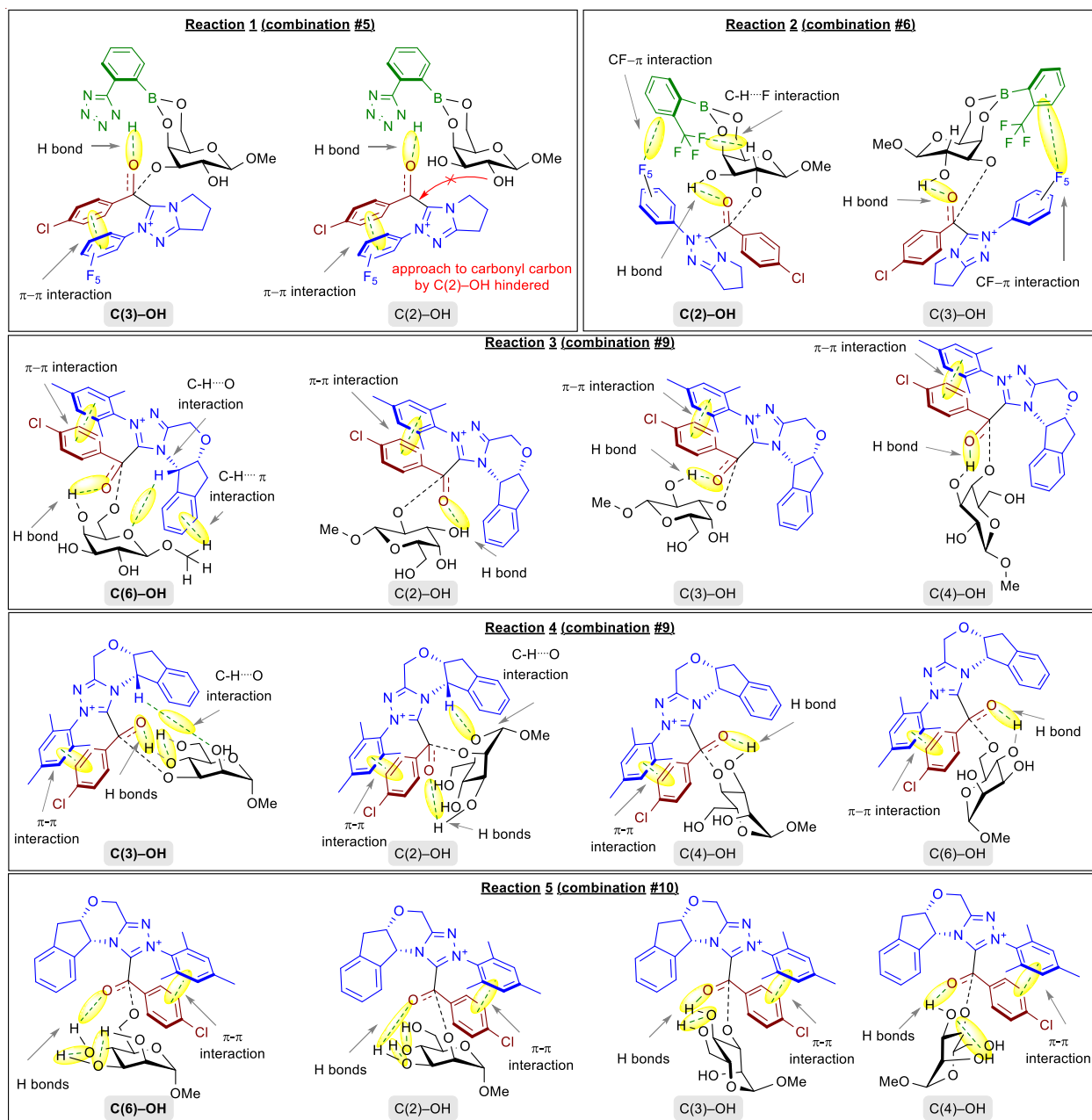
**Figure S39.** Schematic representations of the possible interactions that will occur in the regioselective intermediates and similarly transition states. The major C–OH acylation is in bold for each reaction.

### 3.5. Regio-determining TSs – case study using Reaction 4

To verify that our usage of intermediates as a proxy to the interactions in the corresponding TSs is appropriate, we analyzed the TSs for the regio-determining step in **Reaction 4** (figure S36). The optimized DFT TS structures are given in figure S40. Comparing the TSs with their corresponding intermediates in figure S38, we can see that the same interactions present in the intermediates are also present in the TSs, thus suggesting that the stabilizing interactions giving stable intermediates also possibly stabilize the transition states.

The following TS barriers for **Reaction 4** indicates that C(3)-OH acylation has the lowest activation barrier and is predicted to be kinetically most favorable, consistent with the experimentally observed C(3)-OH acylated product.

| TS_man_N4_B11_O2_Re | TS_man_N4_B11_O2_Si |
|---|---|
| 7.0 kcal mol$^{-1}$ | 1.8 kcal mol$^{-1}$ |
|  |  |
| **TS_man_N4_B11_O3_Re** | **TS_man_N4_B11_O3_Si** |
| 3.1 kcal mol$^{-1}$ | **0.0 kcal mol$^{-1}$** |
|  |  |
| **TS_man_N4_B11_O4_Re** | **TS_man_N4_B11_O4_Si** |
| 10.6 kcal mol$^{-1}$ | 5.2 kcal mol$^{-1}$ |
|  |  |

| TS_man_N4_B11_O6_Re | TS_man_N4_B11_O6_Si |
|:---:|:---:|
| 6.3 kcal mol⁻¹ | 1.4 kcal mol⁻¹ |



**Figure S40.** Optimized TS structures for the regio-determining transition states for the formation of C–O bond in the intermediate in **Reaction 4**. Key bond distances are given in Å. Relative activation barriers are given in kcal mol⁻¹ and taken relative to the lowest activation barrier.

**3.6. Table S6.** Optimized structures and absolute energies, zero-point energies

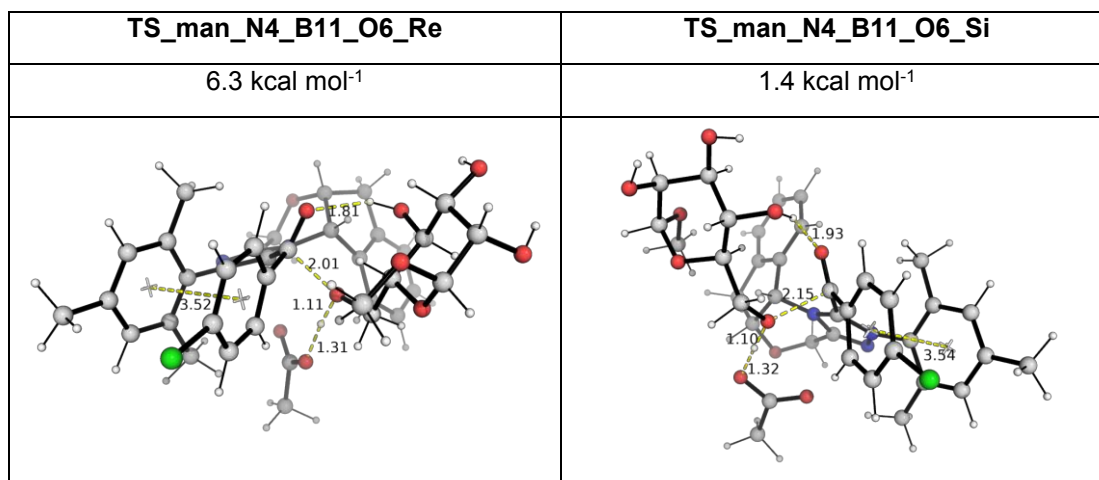Geometries of all optimized structures (in *.xyz* format with their associated energy in Hartrees) are included in a separate folder named *final_xyz_structures*. All these data have been uploaded to zenodo.org (DOI: 10.5281/zenodo.6327868).

Absolute values (in Hartrees) for SCF energy, zero-point vibrational energy (ZPE), enthalpy and quasi-harmonic Gibbs free energy (at 323.15K) for M06-2X/def2-SVP optimized structures are given below. Single point corrections in SMD(acetonitrile) using M06-2X/def2-TZVP functional are also included.

| Structure | E/au | ZPE/au | H/au | T.S/au | qh-G/au | SP M06-2X/def2TZVP |
|---|---|---|---|---|---|---|
| aldehyde_2a | -804.614711 | 0.101454 | -804.5037 | 0.042369 | -804.545817 | -805.1709337 |
| boronic_acid_B1 | -636.582931 | 0.192172 | -636.37469 | 0.057562 | -636.430201 | -637.3348694 |
| H2O | -76.323214 | 0.021594 | -76.297521 | 0.020204 | -76.317725 | -76.43444235 |
| NHC_N1 | -1084.927573 | 0.165762 | -1084.7433 | 0.063464 | -1084.804623 | -1086.209713 |
| AA_N1_c3 | -1888.769838 | 0.260864 | -1888.4813 | 0.085925 | -1888.561962 | -1890.656312 |
| AA_N1_c2 | -1888.775772 | 0.260836 | -1888.4873 | 0.084881 | -1888.567396 | -1890.656851 |
| AA_N1 | -1888.775793 | 0.260793 | -1888.4874 | 0.084921 | -1888.567482 | -1890.65731 |
| glucoside_1 | -725.643582 | 0.228916 | -725.39783 | 0.057656 | -725.454409 | -726.5196905 |
| glucoside_B1_23diol | -1209.552171 | 0.371438 | -1209.1532 | 0.084759 | -1209.232985 | -1210.966597 |
| glucoside_B1_34diol | -1209.54895 | 0.370831 | -1209.1503 | 0.085577 | -1209.230795 | -1210.965661 |
| glucoside_B1_46diol | -1209.568717 | 0.371562 | -1209.1697 | 0.084526 | -1209.249196 | -1210.982336 |
| galactoside | -725.652674 | 0.229552 | -725.40666 | 0.056875 | -725.462639 | -726.5227902 |
| B9 | -664.583683 | 0.154897 | -664.41454 | 0.053859 | -664.466841 | -665.3702877 |
| galactoside_B9_23diol | -1237.543626 | 0.333305 | -1237.1843 | 0.081445 | -1237.261347 | -1238.998131 |
| galactoside_B9_34diol | -1237.548714 | 0.332787 | -1237.1896 | 0.082703 | -1237.267408 | -1239.006574 |
| galactoside_B9_46diol | -1237.569034 | 0.33439 | -1237.2093 | 0.078775 | -1237.284232 | -1239.014657 |
| B10 | -744.489932 | 0.13184 | -744.34411 | 0.052736 | -744.395522 | -745.3714579 |
| galactoside_B10_23diol | -1317.449561 | 0.310053 | -1317.1136 | 0.080815 | -1317.19033 | -1318.998229 |
| galactoside_B10_34diol | -1317.463306 | 0.310522 | -1317.127 | 0.081408 | -1317.20371 | -1319.009917 |
| galactoside_B10_46diol | -1317.475216 | 0.310907 | -1317.139 | 0.079975 | -1317.214353 | -1319.020695 |
| mannoside | -725.64122 | 0.228852 | -725.39554 | 0.057456 | -725.452092 | -726.517678 |

| | | | | | | |
|---|---|---|---|---|---|---|
| INT_gal_N1_B10_O2_Re | -3205.89074 | 0.56323 | -3205.2762 | 0.133772 | -3205.400908 | -3209.21994 |
| INT_gal_N1_B10_O2_Si | -3205.893766 | 0.561634 | -3205.2807 | 0.13518 | -3205.4059 | -3209.230654 |
| INT_gal_N1_B10_O3_Re | -3205.890674 | 0.562229 | -3205.2767 | 0.137606 | -3205.403266 | -3209.22644 |
| INT_gal_N1_B10_O3_Si | -3205.879828 | 0.563202 | -3205.2649 | 0.135125 | -3205.390642 | -3209.212477 |
| INT_gal_N1_B9_O2_Re | -3125.996992 | 0.586357 | -3125.3589 | 0.136407 | -3125.485177 | -3129.224536 |
| INT_gal_N1_B9_O2_Si | -3126.004327 | 0.585693 | -3125.3673 | 0.135464 | -3125.49276 | -3129.232675 |
| INT_gal_N1_B9_O3_Re | -3125.992594 | 0.585915 | -3125.3551 | 0.13613 | -3125.480944 | -3129.230787 |
| INT_gal_N1_B9_O3_Si | -3126.001052 | 0.584743 | -3125.3649 | 0.134511 | -3125.490114 | -3129.232745 |
| INT_gal_N4_B11_O2_Re | -2580.250711 | 0.698388 | -2579.5032 | 0.130524 | -2579.623753 | -2582.824691 |
| INT_gal_N4_B11_O2_Si | -2580.24786 | 0.698512 | -2579.5002 | 0.131113 | -2579.621057 | -2582.820042 |
| INT_gal_N4_B11_O3_Re | -2580.249975 | 0.699057 | -2579.5019 | 0.129462 | -2579.622199 | -2582.823436 |
| INT_gal_N4_B11_O3_Si | -2580.244493 | 0.699531 | -2579.4959 | 0.130745 | -2579.616763 | -2582.820846 |
| INT_gal_N4_B11_O4_Re | -2580.246036 | 0.698219 | -2579.4986 | 0.128967 | -2579.618901 | -2582.819359 |
| INT_gal_N4_B11_O4_Si | -2580.239243 | 0.697611 | -2579.492 | 0.130624 | -2579.613261 | -2582.812778 |
| INT_gal_N4_B11_O6_Re | -2580.266552 | 0.698464 | -2579.5196 | 0.126204 | -2579.638061 | -2582.835848 |
| INT_gal_N4_B11_O6_Si | -2580.251766 | 0.699229 | -2579.5037 | 0.128197 | -2579.623172 | -2582.826279 |
| INT_man_N4_B11_O2_Re | -2580.245541 | 0.697508 | -2579.498 | 0.132607 | -2579.620421 | -2582.823866 |
| INT_man_N4_B11_O3_Re | -2580.24213 | 0.697429 | -2579.495 | 0.130691 | -2579.616371 | -2582.822096 |
| INT_man_N4_B11_O4_Re | -2580.248702 | 0.698415 | -2579.501 | 0.130245 | -2579.621721 | -2582.822366 |
| INT_man_N4_B11_O6_Re | -2580.256535 | 0.698533 | -2579.5089 | 0.130708 | -2579.629701 | -2582.829512 |
| INT_man_N4_B11_O2_Si | -2580.259454 | 0.698493 | -2579.5118 | 0.129824 | -2579.632256 | -2582.832234 |

| | | | | | | |
|---|---|---|---|---|---|---|
| INT_man_N4 _B11_O3_Si | -2580.258888 | 0.698013 | -2579.5116 | 0.130913 | -2579.632655 | -2582.832067 |
| INT_man_N4 _B11_O4_Si | -2580.255714 | 0.698096 | -2579.5082 | 0.132583 | -2579.630093 | -2582.83073 |
| INT_man_N4 _B11_O6_Si | -2580.255623 | 0.698992 | -2579.5079 | 0.127901 | -2579.62715 | -2582.831125 |
| INT_man_N5 _B11_O2_Re | -2580.24795 | 0.698137 | -2579.5004 | 0.130962 | -2579.621589 | -2582.825599 |
| INT_man_N5 _B11_O3_Re | -2580.244282 | 0.697631 | -2579.4971 | 0.130823 | -2579.61835 | -2582.822082 |
| INT_man_N5 _B11_O4_Re | -2580.253342 | 0.698956 | -2579.5055 | 0.128142 | -2579.625152 | -2582.825638 |
| INT_man_N5 _B11_O6_Re | -2580.249624 | 0.698248 | -2579.5021 | 0.131858 | -2579.623538 | -2582.826188 |
| INT_man_N5 _B11_O2_Si | -2580.25843 | 0.698057 | -2579.511 | 0.130152 | -2579.631821 | -2582.83253 |
| INT_man_N5 _B11_O3_Si | -2580.25833 | 0.69756 | -2579.5114 | 0.130902 | -2579.632522 | -2582.831964 |
| INT_man_N5 _B11_O4_Si | -2580.256943 | 0.698314 | -2579.5095 | 0.129624 | -2579.629921 | -2582.832262 |
| INT_man_N5 _B11_O6_Si | -2580.260399 | 0.698206 | -2579.513 | 0.130915 | -2579.63397 | -2582.834486 |
| TS_man_N4 _B11_O2_Re | -2809.076249 | 0.758052 | -2808.2625 | 0.14227 | -2808.395197 | -2811.915257 |
| TS_man_N4 _B11_O3_Re | -2809.080915 | 0.757859 | -2808.2673 | 0.143717 | -2808.400763 | -2811.920635 |
| TS_man_N4 _B11_O4_Re | -2809.07105 | 0.75845 | -2808.2571 | 0.142367 | -2808.38959 | -2811.909957 |
| TS_man_N4 _B11_O6_Re | -2809.076314 | 0.759873 | -2808.261 | 0.144518 | -2808.394092 | -2811.917624 |
| TS_man_N4 _B11_O2_Si | -2809.083887 | 0.758013 | -2808.2701 | 0.143355 | -2808.403344 | -2811.923044 |
| TS_man_N4 _B11_O3_Si | -2809.085262 | 0.758016 | -2808.2714 | 0.145222 | -2808.405577 | -2811.925105 |
| TS_man_N4 _B11_O4_Si | -2809.07664 | 0.759658 | -2808.2612 | 0.145359 | -2808.395015 | -2811.918819 |
| TS_man_N4 _B11_O6_Si | -2809.082656 | 0.759436 | -2808.2678 | 0.143292 | -2808.400629 | -2811.925177 |

## 5. Supplemental references

1. Kerr, M. S., de Alaniz, J. R., and Rovis, T. (2005). An efficient synthesis of achiral and chiral 1,2,4-triazolium salts: bench stable precursors for N-heterocyclic carbenes. J. Org. Chem. *70*, 5725-5728. doi: 10.1021/jo050645n.

2. Wu, Z., and Wang, J. (2017). Enantioselective medium-ring lactone synthesis through an NHC-catalyzed intramolecular desymmetrization of prochiral 1,3-Diols. ACS Catal. *7*, 7647–7652. doi: 10.1021/acscatal.7b02302.

3. Li, Y., and Kluger, R. (2018). Lead-catalyzed aqueous benzoylation of carbohydrates with an acyl phosphate ester. J. Org. Chem. *83*, 7360-7365. doi: 10.1021/acs.joc.7b03142.

4. Rocheleau, S., Pottel, J., Huskić, I., and Moitessier, N. (2017). Highly regioselective monoacylation of unprotected glucopyranoside using transient directing-protecting groups. Eur. J. Org. Chem. *2017*, 646-656. doi: 10.1002/ejoc.201601457.

5. Shibayama, H., Ueda, Y., Tanaka, T., and Kawabata, T. (2021). Seven-step stereo divergent total syntheses of punicafolin and macaranganin. J. Am. Chem. Soc. *143*, 1428-1434. doi: 10.1021/jacs.0c10714.

6. Grimme, S. (2019). Exploration of chemical compound, conformer, and reaction space with meta-dynamics simulations based on tight-binding quantum chemical calculations. J. Chem. Theory Comput. *15*, 2847–2862. doi: 10.1021/acs.jctc.9b00143.

7. Pracht, P., Bohle, F., and Grimme, S. (2020). Automated exploration of the low-energy chemical space with fast quantum chemical methods. Phys. Chem. Chem. Phys. *22*, 7169–7192. doi: 10.1039/C9CP06869D.

8. Bannwarth, C., Ehlert, S., and Grimme, S. (2019). GFN2-XTB - An accurate and broadly parametrized self-consistent tight-binding quantum chemical method with multipole electrostatics and density-dependent dispersion contributions. J. Chem. Theory Comput. *15*, 1652–1671. doi: 10.1021/acs.jctc.8b01176.

9. Grimme, S., Bannwarth, C., and Shushkov, P. (2017). A robust and accurate tight-binding quantum chemical method for structures, vibrational frequencies, and noncovalent interactions of large molecular systems parametrized for all Spd-Block elements ($Z$ = 1-86). J. Chem. Theory Comput. *13*, 1989–2009. doi: 10.1021/acs.jctc.7b00118.

10. Bannwarth, C., Caldeweyher, E., Ehlert, S., Hansen, A., Pracht, P., Seibert, J., Spicher, S., and Grimme, S. (2021). Extended tight-binding quantum chemistry methods. Wiley Interdiscip. Rev. Comput. Mol. Sci. *11*. doi: 10.1002/wcms.1493.

11. Zhao, Y., and Truhlar, D. G. (2008). The M06 suite of density functionals for main group thermochemistry, thermochemical kinetics, noncovalent interactions, excited states, and transition elements: two new functionals and systematic testing of four M06-class functionals and 12 other function. Theor. Chem. Acc. *120*, 215–241. doi: 10.1007/s00214-007-0401-8.

12. Weigend, F., and Ahlrichs, R. (2005). Balanced basis sets of split valence, triple zeta valence and quadruple zeta valence quality for H to Rn: design and assessment of accuracy. Phys. Chem. Chem. Phys. *7*, 3297–3305. doi: 10.1039/B508541A.

13. Weigend, F. (2006). Accurate coulomb-fitting basis sets for H to Rn. Phys. Chem. Chem. Phys. *8*, 1057–1065. doi: 10.1039/B515623H.

14. Frisch, M. J., Trucks, G. W., Schlegel, H. B., Scuseria, G. E., Robb, M. A., Cheeseman, J. R., Scalmani, G., Barone, V., Petersson, G. A., and Nakatsuji, H. et al. Gaussian 16, Revision B.01. 2016.

15. Marenich, A. V., Cramer, C. J., and Truhlar, D. G. (2009). Universal solvation model based on solute electron density and on a continuum model of the solvent defined by the bulk dielectric constant and atomic surface tensions. J. Phys. Chem. B *113*, 6378–6396. doi: 10.1021/jp810292n.

16. Luchini, G., Alegre-Requena, J. V., Funes-Ardoiz, I., and Paton, R. S. (2020). GoodVibes: automated thermochemistry for heterogeneous computational chemistry data. *F1000Research 9*, 291. doi: 10.12688/f1000research.22758.1.

17. Grimme, S. (2012). Supramolecular binding thermodynamics by dispersion-corrected density functional theory. Chem. Eur. J. *18*, 9955–9964. doi: 10.1002/chem.201200497.

18. Schrödinger, L. *The PyMOL molecular graphics development component, Version 1.8*; 2015.

19. Kitaoka, M., Sasaki, T., and Taniguchi, H. (1993). Conversion of sucrose into laminaribiose using sucrose phosphorylase, xylose isomerase and laminaribiose phosphorylase. J. Jpn. Soc. Starch Sci. *40*, 311–314. doi: 10.5458/jag1972.40.311.

Full reference for Gaussian software:

Gaussian 16, Revision B.01, Frisch, M. J.; Trucks, G. W.; Schlegel, H. B.; Scuseria, G. E.; Robb, M. A.; Cheeseman, J. R.; Scalmani, G.; Barone, V.; Mennucci, B.; Petersson, G. A.; Nakatsuji, H.; Caricato, M.; Li, X.; Hratchian, H. P.; Izmaylov, A. F.; Bloino, J.; Zheng, G.; Sonnenberg, J. L.; Hada, M.; Ehara, M.; Toyota, K.; Fukuda, R.; Hasegawa, J.; Ishida, M.; Nakajima, T.; Honda, Y.; Kitao, O.; Nakai, H.; Vreven, T.; Montgomery Jr., J. A.; Peralta, J. E.; Ogliaro, F.; Bearpark, M.; Heyd, J. J.; Brothers, E.; Kudin, K. N.; Staroverov, V. N.; Kobayashi, R.; Normand, J.; Raghavachari, K.; Rendell, A.; Burant, J. C.; Iyengar, S. S.; Tomasi, J.; Cossi, M.; Rega, N.; Millam, J. M.; Klene, M.; Knox, J. E.; Cross, J. B.; Bakken, V.; Adamo, C.; Jaramillo, J.; Gomperts, R.; Stratmann, R. E.; Yazyev, O.; Austin, A. J.; Cammi, R.; Pomelli, C.; Ochterski, J. W.; Martin, R. L.; Morokuma, K.; Zakrzewski, V. G.; Voth, G. A.; Salvador, P.; Dannenberg, J. J.; Dapprich, S.; Daniels, A. D.; Farkas, Ö.; Foresman, J. B.; Ortiz, J. V; Cioslowski, J.; Fox, D. J. Gaussian, Inc., Wallingford CT, 2016.